Annals of R.S.C.B., ISSN:1583-6258, Vol. 25, Issue 6, 2021, Pages. 14801 - 14819
Received 25 April 2021; Accepted 08 May 2021.

Phytosynthesis of Cobalt Ferrite Nanoparticles by Crude Extract of *Rheum Ribes*.

Maryam Mohammed Hussein M. Jawad*, Raghad DHyea Abdul Jalill*, Ahmed Majeed Al‑Shammari**, Ahmed N. Abd***.
*Department of Biology/ College of Science/ AL-Mustainsiriyah, University/ Baghdad /Iraq.** Experimental Therapy Department, Iraqi Centre for Cancer and Medical Genetic Research, Mustansiriyah. University, Baghdad /Iraq. *** Department of Physics / College of Science/ AL-Mustainsiriyah.
Corresponding author: Dr. Raghad DHyea Abdul Jalill, Cellphone: 07700032312.
Email: stru@uomustansiriyah.edu.iq, raghadalshybany@ymail.com.

Abstract

The objective of this study was identifying the flavonoids in Rhizomes of Iraqi *Rheum ribes* and utilization these extract to phytosynthesis of cobalt ferrite nanoparticles with characterization of them. The results obtained from the HPLC analysis indicate that rhizomes of Iraqi *R. ribes* contain seven compounds of flavonoids which include: 1.735 µg/g aloe-emodin, 24.966 µg/g emodin, 5.533 µg/g chrysophanol, 17.542 µg/g physician, 4.242 µg/g rhein and 15.873 µg/g rutin,.

Plant extract-mediated cobalt ferrite nanoparticles were characterized by various techniques to analyze the size, shape, crystallinity. Their average size (which calculated by AFM) were: (100.36, 68.80, 69.01) nm for (1, 2 and 3) procedures, respectively. While procedure 4 was fail to produce nanoparticles, their average size was (192.38 nm). From SEM study, it is confirmed that the particles are almost spherically shaped and uniformly arranged.

The FTIR results showed strong bands are observed in (procedure 4) around 585- 400 cm−1 confirm the presence of CoFe2O4 nanoparticles while other procedures showed tetrahedral metal stretching ν(Fe-O tetra) and octahedral metal stretching ν(Co-O) bond.

The XRD patterns of all samples indicate spinel cobalt ferrite magnetic nanoparticles having face centered cubic structure. This structure was pure in procedure 1. The average crystallite size of nanoparticles was calculated by Scherer's equation, they were: (47.41, 45.1, 50.62 and 44 nm) nm. The results of UV–visible spectral of procedures (1-4) showed that the absorption spectra of phytosynthesis NPs exhibit strong absorption at 221 nm. More than one band gaps of each sample (3.4 eV and 4.5 eV). These two energy gaps are indicating to presence of a quantum well. These results follow quantum laws.

Keyword:
Cobalt ferrite; HPLC; Nanoparticles; Phytosynthesis, *Rheum ribes*.

Introduction

Rheum ribes L. is an Iraqi species belong to the family Polygonaceae, (Tanrikut *et al.*, 2013). It is found in eastern Turkey on dry mountain slopes, Syrian and in other related local areas. The edible part of the plant is the flowering stem, which is eaten raw salads or cooked soups in south west Asian countries, they considered it as one of the most important sources of crude drug in folk medicine (Andıç *et al.*, 2009), (Tartık *et al.*, 2015).

The young shoots contain vitamins A, B, C and tannins (8 %) and anthracene derivatives (0.025 %) (Andiç *et al*. 2009). A variety of constituents have been separated from rhizomes and

Annals of R.S.C.B., ISSN:1583-6258, Vol. 25, Issue 6, 2021, Pages. 14801 - 14819
Received 25 April 2021; Accepted 08 May 2021.

roots, they belong to such classes as anthraquinone, stilbenes and essential oils (Wang *et al.*, 2012; Liu *et al.*, 2009). It also, contain a wide variety and different concentration of phenolic and Flavonoids constitutes: chrysophanol, physcion, Rhein, aloe-emodin, physcion-8-O-glucoside, aloe-emodin-8-Oglucoside, rhaponticin (Tuzlacı *et al.*, 1991), stilbenoids and anthraquinones (Uyar *et al*., 2014), butylated hydroxyanisole (BHA), butylated hydroxytoluene, and tert-butylhydroquinone (Grice H.C., 1988; Wichi H.P., 1986), sennoside A (Tuzlaci and Mericli, 1992) and rhaponticin (Mericli and Tuzlaci, 1990).

A nanoparticle or ultrafine particle is a particle of matter that is between 1 and 100 nanometres (nm) in diameter. Nanoparticles have a great outstanding scientific concern as they bridge the gap between bulk materials and atomic or molecular structures (Thakkar *et al.*, 2010). The properties of nanoparticles often differ markedly from those of larger particles of the same substance.

Cobalt Ferrite oxide ($CoFe_2O_4$) NPs is one of the most interesting metal oxide nanoparticles (jia *et al.*, 2012). They have unique physical properties such as: high Curie temperature, large magneto crystalline anisotropy, high magneto-strictive coefficient, mechanical hardness, good coupling efficiency, and high magnetostriction, high coactivity, low dielectric constant, moderate saturation magnetization, good physical and chemical stability, (jia *et al.*, 2012), high magnetocrystalline anisotropy, and high intrinsic magnetocrystalline anisotropy at room temperature (Routray *et al.*, 2018; Andersen and Christensen, 2015; Lu *et al.*, 2015; Gore *et al.*, 2017; Varma, *et al.*, 2008; Tran and Webster, 2010). Additionally, the particles less than 10 nm in size, the superparamagnetic behavior is observed to increase with a decrease in particle size (Yáñez-Vilar *et al.*, 2009). $CoFe_2O_4$ NPs have a great potential for various applications and engineering including: magnetic recording, industries, and packaging accessories, magnetic energy storage, catalysis, and waste water treatment (Issa *et al.*, 2013; Pathak and Pramanik, 2011; Wang and Sun, 2007; Mathew and Juang, 2007; Wang *et al.*, 2016).

Recent studies revealed their biomedical applications such as: antimicrobial activity against multidrug resistant bacterial strains (Brigger *et al.*, 2002), anticancer activities (Park *et al.*, 2015); (Ansari *et al.*, 2016), drug delivery technique, (Dey *et al.*, 2018). Cobalt ferrite nanoparticles can be prepared via chemical and physical approaches (Prabhakaran and Hemalatha, 2016; Rana *et al.*, 2010; Tatarchuk *et al.*, 2017). There is a need to improve an eco-friendly avenue for synthesis of nanomaterial that does not use toxic chemicals in the synthesis protocol, and to minimize or eliminate the use of environmental-risk substances, toxic chemical species and expensive surfactants (Dang *et al.*, 2012). Accordingly, it became possible to synthesize nanoparticles by means of various biological methods, which include the use of plants extract or even their metabolism products, these procedures are generally called green synthesis or phytosynthesis (Marslin *et al.*, 2018). Okra extract could synthesize single-phase crystalline structures of CoFe2O4 nanoparticles with size from (45-55) nm, (Kombaiah *et al.*, 2018). In addition, Mangifera indica leaf extract succeeded in forming of smooth surface, cubic and pentagonal cobalt nanoparticles with an average size of (25-40) nm, a (Okwunodulu *et al.*, 2019). Several factors affect the synthesis, characterization and the nucleation and subsequent formation of stabilized nanoparticles in addition to the type of the adsorbate and the activity of the catalysts used in the synthesis process (Somorjai and Park, 2008). Some of the important factors are: pH, reaction time, and temperature (Baker *et al.*, 2013) in addition to plant extract concentrations, bulk material concentrations. The objective of this study was identifying the flavonoids in

Annals of R.S.C.B., ISSN:1583-6258, Vol. 25, Issue 6, 2021, Pages. 14801 - 14819
Received 25 April 2021; Accepted 08 May 2021.

Rhizomes of Iraqi *Rheum ribes* and utilization these extract to phytosynthesis of cobalt ferrite nanoparticles with characterization of them.

Materials and procedures

Extraction of *R. ribes* crude extract.

Rhizomes of *Rheum ribes* was purchased from the local market and authenticated by the Herbarium of Iraqi Ministry of Health according to a taxonomic procedure as *Rheum ribes*; belong to the plant family Polygonaceae. After cleaning and milling, a crushed Rhizomes was kept in a dark glass bottles in refrigerator.

Methanol extraction of *R. ribes* crude extract

One gram of above plant powder was dissolved in 20 ml hexane to remove fat layer, then the organic layer dissolved 100 ml of 80:20 (methanol: water). The extract was subjected to ultra-sonication at 60 % duty cycles for 25 min at 25°C followed by centrifugation at 7500 rpm for 15 min. The clear supernatant of each sample was subjected to charcoal treatment to remove pigments prior to evaporation under vacuum.

Analysis of active ingredient in crude extract

Equipment

The separation occurred on liquid chromatography Shimadzu 10AV-LC equipped with binary delivery pump model LC-10A shimadzu, the eluted peaks were monitored by UV-Vis 10 A-SPD spectrophotometer. The main listed compounds were separated under the optimum condition Column: phenomenex C-18 ,3 µm particle size (50 x 2.0 mm I.D) column, Mobile phase: linear gradient of, solvent A 0.1% phosphoric acid solvent B was (6:3:1, v/v) of acetonitrile: methanol: 0.1% phosphoric acid, linear gradient program from 0%B to 100% B for 10 minutes. Flow rate 1.0 ml/min. Detection: UV 280 nm.

Preparation of standard compounds:

Dissolve 10 mg of each of following standard compounds in 10 ml of distilled water. Five-fold dilutions were used to produce a decimal dilution series. The standard compounds were: (Rhein, Rutin, Emodin, Aloe –emodin, Chrysophanol, Physcion).

Injection of *R. ribes* crude extract in HPLC

Dried samples were re-suspended in 1.0 ml HPLC grade methanol by overtaxing, the mixture was passed through 2.5 µm disposable filter, and stored at 4°C for further analysis, then 20 µl of the sample injected into HPLC system according the optimum condition.

Calculation:

Concentration of sample (ug/ml) = (Area of sample of sample/ Area of standard) * concentration of standard x dilution Factor

Table (1): The retention time (RT) and area under curves of reference standard compounds.

No.	RSt.	R.T (min.)	Aru. (µvolt)	Con.
1	Aloe -emodin	1.085	130251	13.84
2	Emodin	2.252	126439	13.434

Annals of R.S.C.B., ISSN:1583-6258, Vol. 25, Issue 6, 2021, Pages. 14801 - 14819
Received 25 April 2021; Accepted 08 May 2021.

3	Chrysophanol	3.502	100380	10.666
4	Physcion	4.322	116612	12.39
5	Rhein	5.17	126287	13.418
6	Rutin	6.077	233077	24.765

RSt.: reference standard; R.T: retention time in minuet; Aru.: area under curves (µvolt); Con.; concentration.

Phytosynthesis of $CoFe_2O_4$ NPs by Rhizomes of crude extract of *R. ribes*.

1. Preparation of $CoFe_2O_4$ bulk particles

Black powder pigment powder of bulk CoFe2O4 bulk particles procured from Chemical Book. Molecular weight was 234.62 g/mol and monoisotopic mass: 234.782728. Density 5.3 g/cm3, their average size was >5 micro meter (> 5000 nm). Purity: 99.5 %min. Distil water was used to make solution of (10 mg/ml) concentrations.

2. Phytosynthesis

These were done using two procedure:

- **Procedure 1 and 2:** This was done by adding 1 ml of methanol crude plant extract to (1 mL, 0.1 M) of bulk $CoFe_2O_4$ particles in flask contain 15 ml distal water. Each mixture placed in magnetic stirrer hot plate at (60 and 90) Cº for (3 and 9) hours respectively.
- **Procedure 3 and 4:** This was the same above procedure but the flask contains 25 ml distal water. The degrees were (60 and 90) Cº for (3 and 9) hours respectively.

The Revolutions per minute was 1000 rpm /second. The solutions allowed to cool at room temperature and repeated centrifugations at 15,000 rpm for 10 min. The supernatant was neglected. The precipitate formed was washed with double distilled water and then centrifuged at 1500 rpm for 10 min, (Abdul Jalill, 2018). This was repeated three times. The obtained precipitate (nanopawder) was dried at room temperature for 24 h. and characterized as described fallowing. The conditions synthesises were appeared in in table (1).

3. Characterizations

The fallowing techniques were using to measure the exact pattern of the fabricated, morphology of crystals structure average, phase purity, particle size, and distribution particle.

- **Atomic force microscopy (AFM):** The surface topography, granularity volume distribution and size of biosynthesized nanoparticles was characterized by Atomic Absorption Spectroscopy. A slim film of the sample was prepared on a glass slide, by dropping 100 µl of the sample on the slide. Permitted to dry for 10 min. Then the slides were scanned with AFM, (AA-680, Shimadzu-Japan), (characterized by Dr. Abdul Kareem Al-Samaraii Lab. Baghdad Iraq (Naveen, *et al*., 2010).
- **UV–visible analysis:** The UV–VIS absorption spectra of biosynthesized nanoparticles were recorded by a spectrophotometer. The (bio reduction of the $CoFe_2O_4$ NPs), was monitored by periodic sampling of aliquots (1 mL) of the aqueous component after two times dilution and measuring the UV–VIS spectrum of the solution. UV–VIS spectra of these aliquots were monitored as a function of time of reaction on a Schimadzu 1601 spectrophotometer in 200–800 nm range operated at a resolution of 1 nm (Ba-Abbad *et al*., 2012).

Annals of R.S.C.B., ISSN:1583-6258, Vol. 25, Issue 6, 2021, Pages. 14801 - 14819
Received 25 April 2021; Accepted 08 May 2021.

The absorption coefficient (α) was determined from the optical spectrum using the formula, (Pannaparayil *et al*., 1988):

$$\alpha = 2.3026\ A/t$$

Where: (A) and (t)are the measured absorbance and thickness of the sample, respectively.

The optical bandgap energy (Eg) was evaluated from the absorption spectrum and the optical absorption coefficient (α) near the absorption edge is given by following equation, (Wang and Herron, 1991):

$$\alpha h\nu = B\left(h\nu - E_g\right)^n$$

Where: h, ν, B, and Eg are Plank's constant, frequency of incident photons, constant, and optical band gap energy respectively. Energy gap of CoFe2O4 NPs (Eg) was estimated by plotting hν versus $(\alpha h\nu)^{1/2}$ according Tauc plot, (Tauc, 1974).

X-ray diffraction: X-ray diffraction (XRD) was used to confirm the crystal structure (crystal phases and to determine the crystallite size of each Phase) of (Biosynthetic $CoFe_2O_4$ nanoparticles) . XRD analysis was performed using an X-ray diffractometer with Cu-Kα crystal radiation (λ = 1.54A°)) scanning at a rate of ($5^\circ/min^{-1}$) for (2θ) range of (20º-70 º). The diffraction peaks of samples were identified by comparison with ((JCPDS card no. 77-0426), according to 2θ. (Raval *et al*., 2013). The full width at half maximum (FWHM) was used to determine the crystallite size using Scherer's equation, (Cullity, 1974):

$$\mathbf{t = k\,\lambda / \beta\cos\theta}$$

Where: **t**: is the crystallite size (in nm), **K**: (=0.9) was the Scherer's constant, **λ** is the x-ray wavelength, **β** is (FWHM) (in radian) and **θ** the Bragg's diffraction angle (in degree).

The strain value η and the dislocation density δ value can be evaluated by using the relations in the fallowing equations:

$$\eta = \frac{\boldsymbol{\beta}\cos\boldsymbol{\theta}}{\mathbf{4}} \quad \text{(Wei } et\ al.\text{, 2011)}$$

$$\delta = \frac{\mathbf{1}}{\boldsymbol{G_s}^{\mathbf{2}}} \quad \text{(Jobst } et\ al.\text{, 2013)}$$

- **FTIR analysis**

The surface nature of samples was qualitatively assessed by using FTIR spectroscopy which show that the vibration spectrum of the infrared region, in the range between 4000-400cm-1 using KBr pellet method.

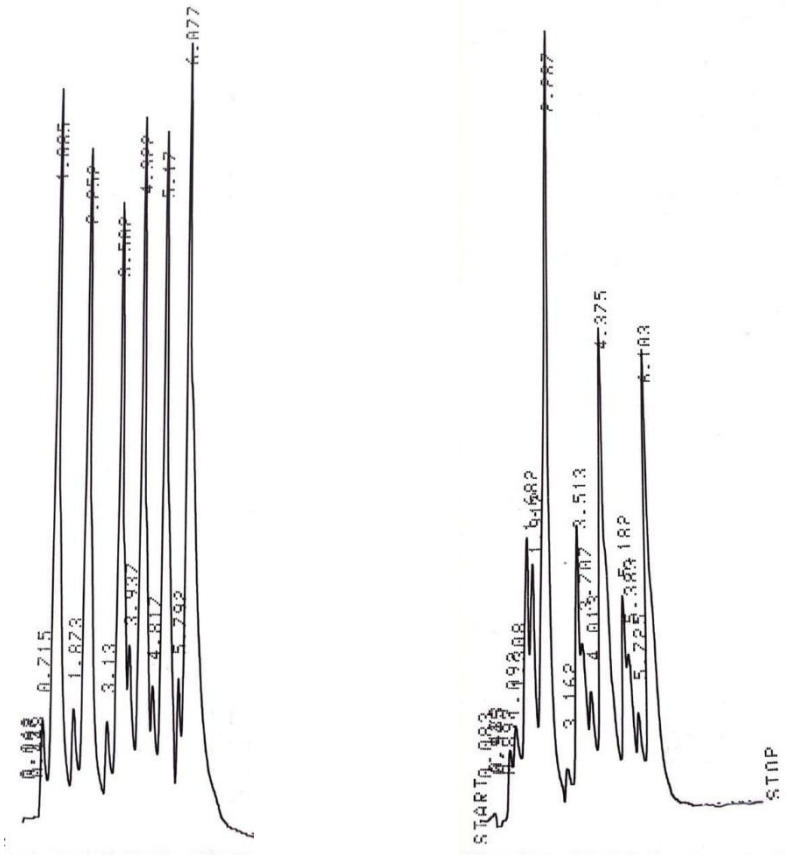
- **SEM analysis**

$CoFe_2O_4$ biosynthetic nanoparticles were analysis by scanning electron microscope (SEM), Vega Tescan (USA), in Centre of Nanotechnology and Advanced Materials/ University of Technology/ Iraq. SEM samples were prepared according to standard procedures of Centre of Nanotechnology and Advanced Materials/ University of Technology/ Iraq.

Annals of R.S.C.B., ISSN:1583-6258, Vol. 25, Issue 6, 2021, Pages. 14801 - 14819
Received 25 April 2021; Accepted 08 May 2021.

Results and Discussion

The column chromatographic separations led to the purification six pure compounds (Fig. 1). As shown in Table (1), the HPLC analysis found that Emodin was most abundant (38.25 %) (24.966 µg/ml), followed by Physcion (29.145 %) (17.542 µg/ml), Rutin (13.193 %) (15.873 µg/ml), Rhein (6.53 %) (4.242 µg/ml) and Aloe -emodin (2.58 %) (1.735 µg/ml).



(A) (B)

Figure (1): HPLC Analysis of: (A) standard flavonoids, (B) Rhizomes of *R. ribes* crude extract.

Table (2): The retention time (RT) and area under curves of *R. ribes* crude extract.

No.	Comp.	R.T (min.)	Aru. (µvolt)	%	Con. (µg/ml)
1	Aloe -emodin	1.092	10587	2.58	1.735
2	Emodin	2.287	152228	38.25	24.966
3	Chrysophanol	3.513	32507	10.289	5.533
4	Physcion	4.375	106965	29.145	17.542
5	Rhein	5.182	25982	6.53	4.242
6	Rutin	6.103	96783	13.193	15.873

Comp.: compound; R.T: retention time in minuet; Aru.: area under curves (µvolt); Con.: concentration.

Annals of R.S.C.B., ISSN:1583-6258, Vol. 25, Issue 6, 2021, Pages. 14801 - 14819
Received 25 April 2021; Accepted 08 May 2021.

Phytosynthesis of $CoFe_2O_4$ NPs by Rhizomes of crude extract of *R. ribes*.

Four procedures were used to synthesis $CoFe_2O_4$ nanoparticles. Methanol crude plant extract was used in procedures (1 to 4).

The results found that three of four procedures were success to produce $CoFe_2O_4$ in nano size, there are: (1, 2, 3) procedures, while procedure 4 was fail to produce nanoparticles, it could not reach lower than 100 nanometer which is the prerequisite for being nanoscale. The following paragraphs is explaining the characterizations in some details:

Atomic force microscopy

The calculated NPs sizes were measured using the software of the AFM. Their average sizes were: (100.36, 68.80, 69.01) nm for (1, 2 and 3) procedures, respectively. While procedure 4 was fail to produce nanoparticles, their average size was (192.38 nm), (Figure 1: A to D).

Their Roughness average (Ra) were: (8.37, 9.15 and 22.9) nm, Root mean square (Sq) were: (9.91, 10.8 and 26.7) nm for (1, 2 and 3) procedures, respectively. (Figure 2: A to d) showed AFM topographic images of phytosynthesis nanoparticles.

SEM Analysis

The scanning electron microscopy was carried out to study the morphology and particle size of the prepared particles. In SEM image of (1 to 4) procedures (Figure 3: A to D), it can be seen that the particles are almost spherically shaped and uniformly arranged

FTIR spectroscopic

In procedure 1, the results of FTIR spectroscopic which appear in figure (3) showed that the samples exhibited very wide strong interye band located near 524.64 cm- and 501.49 cm-, which assigned to ν(Fe-O tetra), addition to medium intense band at 435.91, 459.6, 478.35, 447.48, 416.62 cm-1 attributed to octahedral ν(Co-O),

Procedure 2, showed that the samples exhibited absorption peaks located near 526.49. 482.2, 497.63, 459.06, 439.77, 408.91 cm-, which give an indication of presence tetrahedral metal stretching ν(Fe-O tetra) and octahedral metal stretching ν(Co-O) bond respectively. While procedure 3 showed 526.49 cm- as a very strong peak attributed to ν(Fe-O tetra), in addition to medium intense band at 459.06, 482.2, 497.63, 435.91, 408.91 cm-1 attributed to ν(Co-O octa),

In Procedure 4: the strong bands are observed around 585- 400 cm−1 confirm the presence of CoFe2O4 nanoparticles. The absorption band 536.21 cm-1 corresponds to intrinsic stretching vibration of metal cations at the tetrahedral site stretching ν(Fe-O tetra), while the band 489.92, 451.34, 443.63 and 405.05 cm-1 corresponds to metal cations at the octahedral sites ν(Co-O).

X-ray diffraction:

In Procedure 1: The X-ray diffraction patterns displays sharp and strong reflections which could be indexed on the basis of pure spinel cobalt ferrite magnetic nanoparticles having face centered cubic structure. The planes with h k l values were: (220), (311) and (400). Their average crystallite size of nanoparticles was calculated by Scherer's equation, they were 47.41nm, (Table 2).

In Procedure 2: X-ray diffraction (XRD) of CoFe2O4 reveals abundant information about the crystalline phase, lattice parameter X- ray (theoretical) density, etc. of the prepared material. The obtained XRD peaks shown in figure (3) are indexed using JCPDS card no. 22-1086. The sharp peaks concerning to the reflection planes (220), (311), (222), (400), (422), (511) and (440) in the

Annals of R.S.C.B., ISSN:1583-6258, Vol. 25, Issue 6, 2021, Pages. 14801 - 14819
Received 25 April 2021; Accepted 08 May 2021.

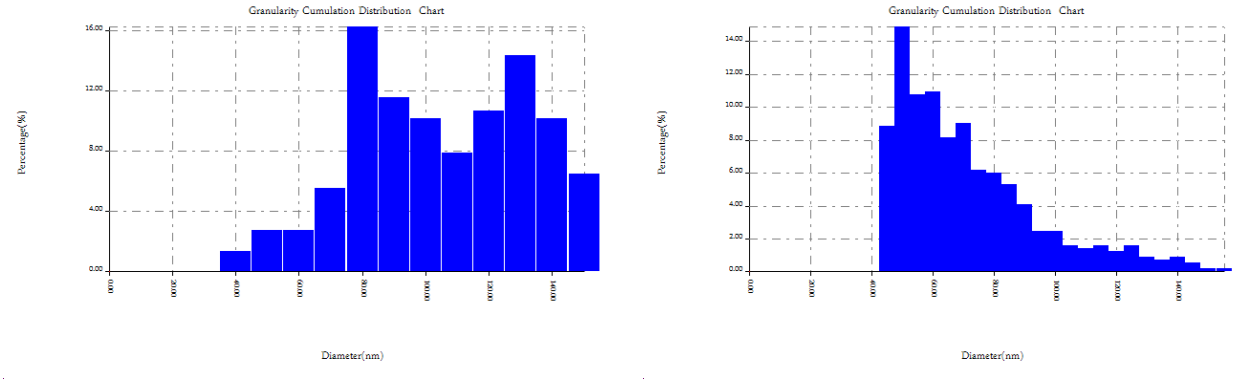
XRD pattern confirm the formation of the cubic spinel structure the average crystallite size of nanoparticles was calculated by Scherer's equation, they were 45.1 nm.

In Procedure 3: the XRD pattern reveals that the nanoparticles are of single phase. Non impurity peak was observed in XRD pattern ensuring the purity of the sample. It was confined that all the peaks of CoFe2O4 NPs matches well with the JCPDS card number (22-1086) that was used to index all the peaks in XRD pattern. The planes with h k l values of (220), (311) and (400), the XRD pattern clearly endorsed to the presence of spinel structure and cubic symmetry. The particle size was calculated and found to be equal to 50.62 nm from the full width half maximum of the strongest peak (311) at $2\theta = 35.343$.

In Procedure 4: the XRD pattern confirms that $CoFe_2O_4$ formed with space group Fd-3m and a spinel structure. The sharp diffraction peak indicates that the crystal phase of $CoFe_2O_4$ is relatively complete. The diffraction peaks around 30.918°, 35. 35° and 57.62° are attributed to the reflections of the (220), (311) and (511) planes of $CoFe_2O_4$, respectively (JCPDS card no.22-1086). The average crystallite size of $CoFe_2O_4$ calculated using Scherrer's formula was approximately 44 nm.

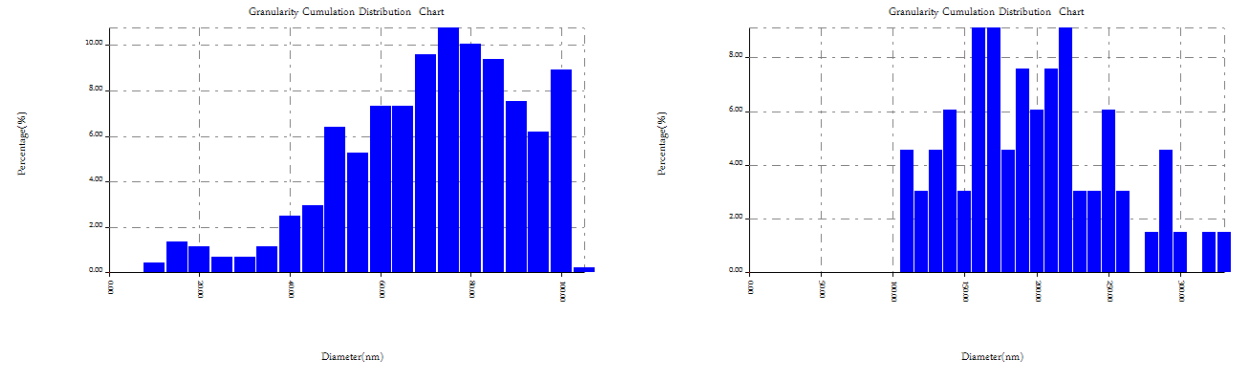
UV–visible analysis

Ultraviolet –visible absorption spectroscopy is a powerful technique to explore the optical properties of nanoparticles. The results of UV–visible spectral of procedures (1-4) showed that the absorption spectra of phytosynthesis NPs exhibit strong absorption at 221 nm. More than one band gaps of each sample (3.4 eV and 4.5 eV), (Figure 4: A to B). These two energy gaps are indicating to presence of a quantum well. The quantum laws explain these results. These results are similar to the result of (Singh *et al*., 2017).



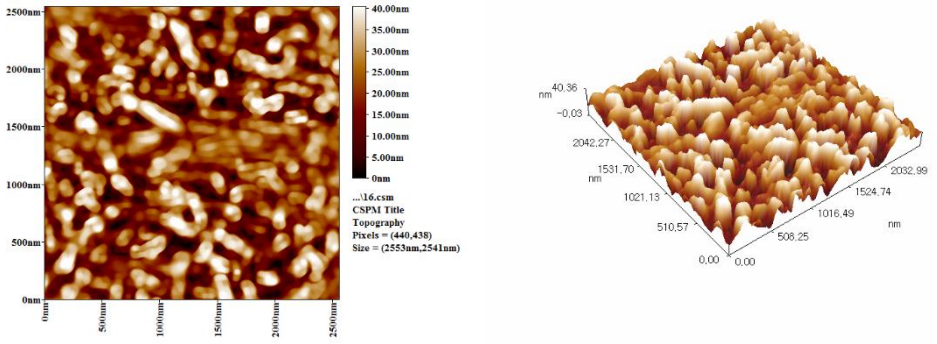
(A) Procedure 1 **(Avg. Diameter:100.36 nm**) **(B)** Procedure 2 (**Avg. Diameter:68.80 nm)**

Annals of R.S.C.B., ISSN:1583-6258, Vol. 25, Issue 6, 2021, Pages. 14801 - 14819
Received 25 April 2021; Accepted 08 May 2021.

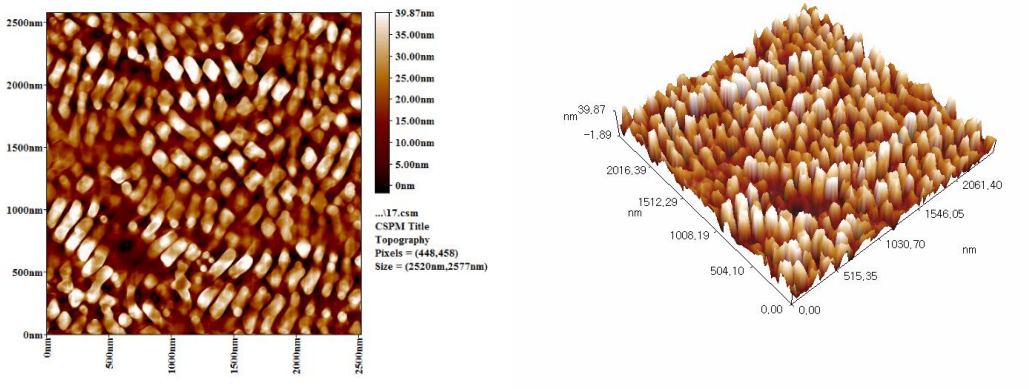


(C) Procedure 3 (**Avg. Diameter:69.01 nm**) **(D)** Procedure 4 (**Avg. Diameter:192.38 nm**)

Fig. (1): Granularity volume distribution chart of CoFe2O4 NPs synthesis by by procedure (1 to 4) of crude plant extract.

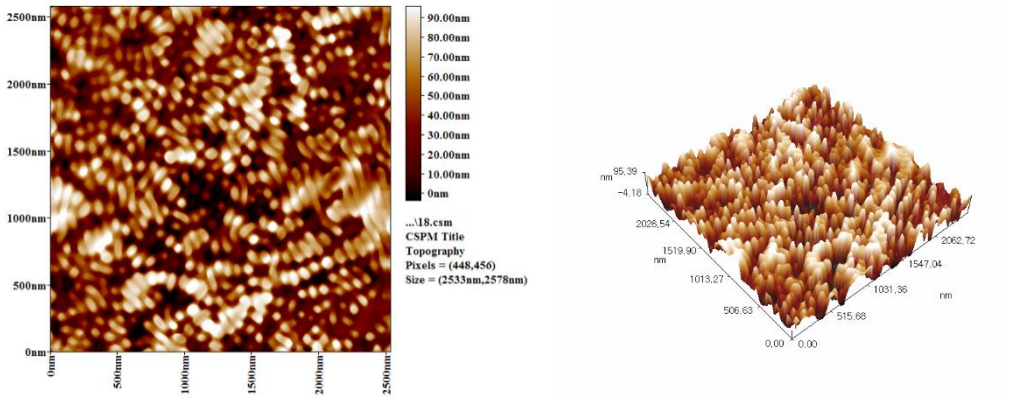


(A) Procedure 1 **(**Roughness average (8.37 nm) and Root mean square (9.91 nm)

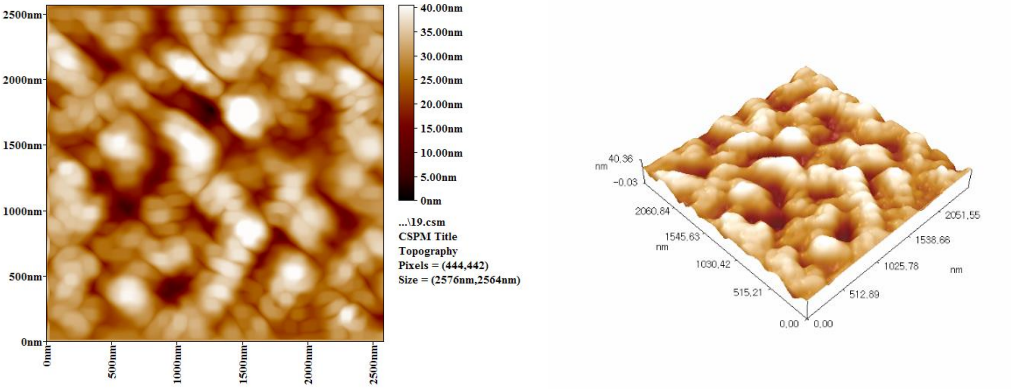


(B) Procedure 2 Roughness average (9.15 nm) and Root mean square (10.8 nm)

Annals of R.S.C.B., ISSN:1583-6258, Vol. 25, Issue 6, 2021, Pages. 14801 - 14819
Received 25 April 2021; Accepted 08 May 2021.

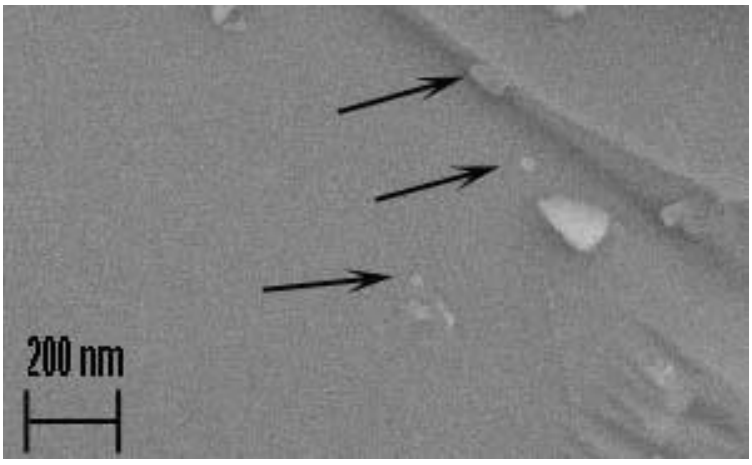


(C) Procedure 3 Roughness average (22.9 nm) and Root mean square (26.7 nm)



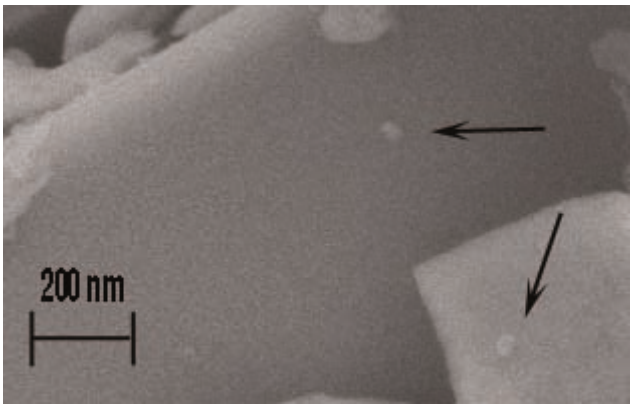
(D) Procedure 4 Roughness average (5.15 nm) and Root mean square (6.43 nm)

Fig. (1): AFM topographic images of $CoFe_2O_4$ NPs synthesis by procedure (1 to 4) of crude plant extract.

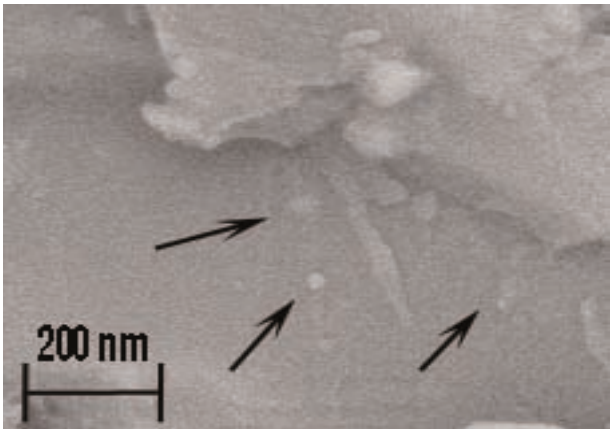


(A) Procedure 1 **()**
عينة رقم 16

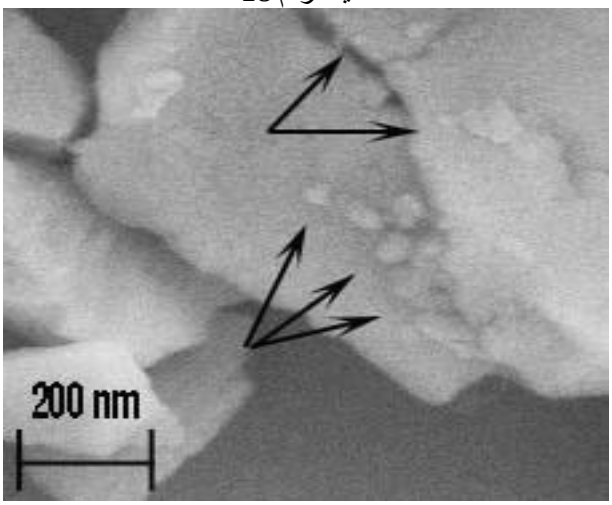
Annals of R.S.C.B., ISSN:1583-6258, Vol. 25, Issue 6, 2021, Pages. 14801 - 14819
Received 25 April 2021; Accepted 08 May 2021.



(B) Procedure 2 ()
عينة رقم 17



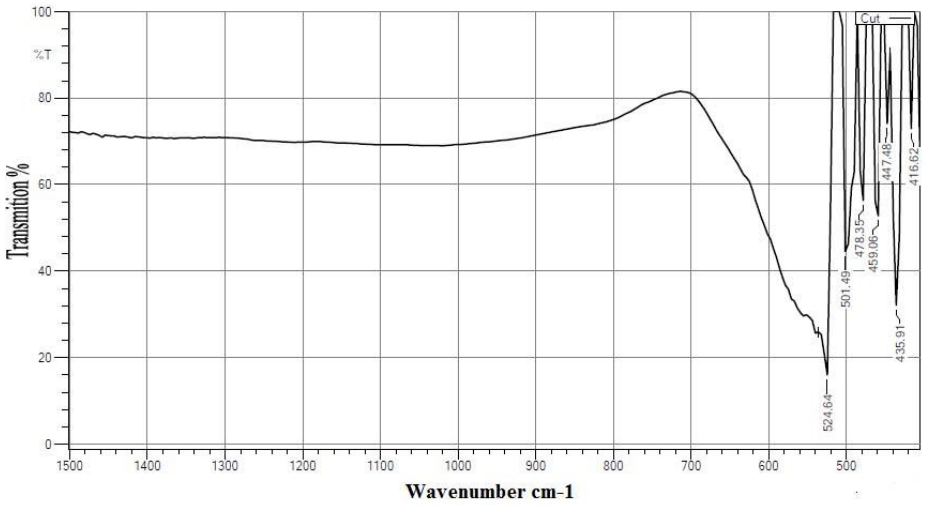
(C) Procedure 3 ()
عينة رقم 18



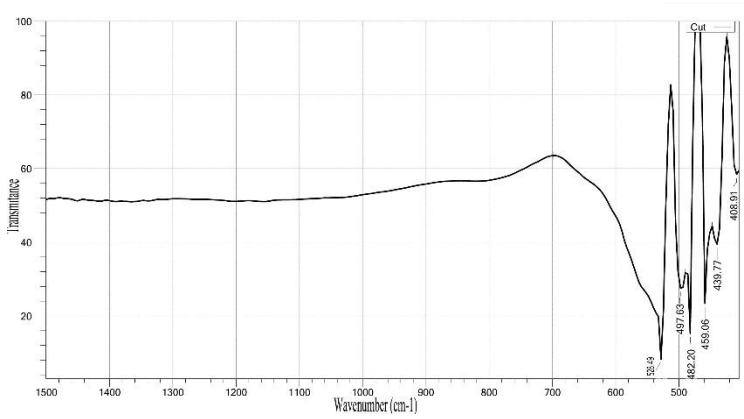
(D) Procedure 4 ()
عينة رقم 19

Fig. (2): SEM image of $CoFe_2O_4$ Phytosynthesis NPs using procedure (1 to 4) of crude plant extract.

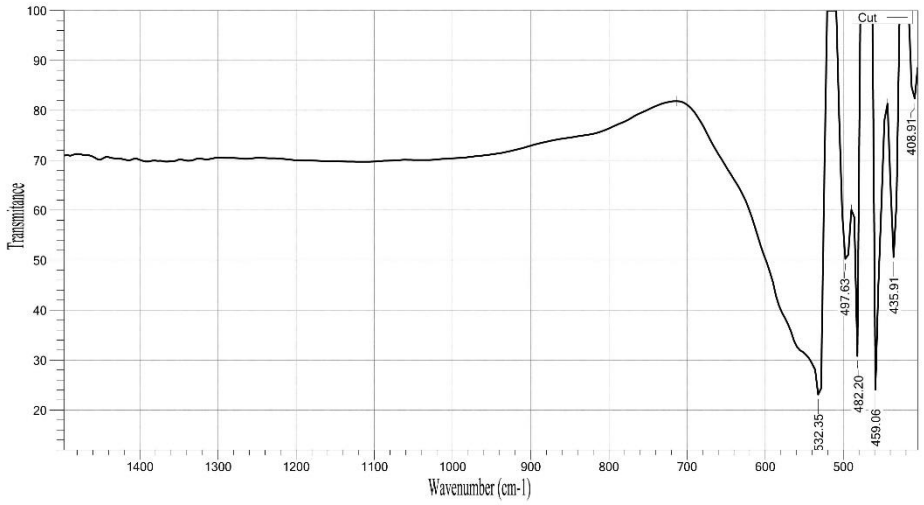
Annals of R.S.C.B., ISSN:1583-6258, Vol. 25, Issue 6, 2021, Pages. 14801 - 14819
Received 25 April 2021; Accepted 08 May 2021.



(A) Procedure 1 **(**strong peck: 524.64, 435.91, 501.49, 459.6, 478.35, 447.48, 416.62)

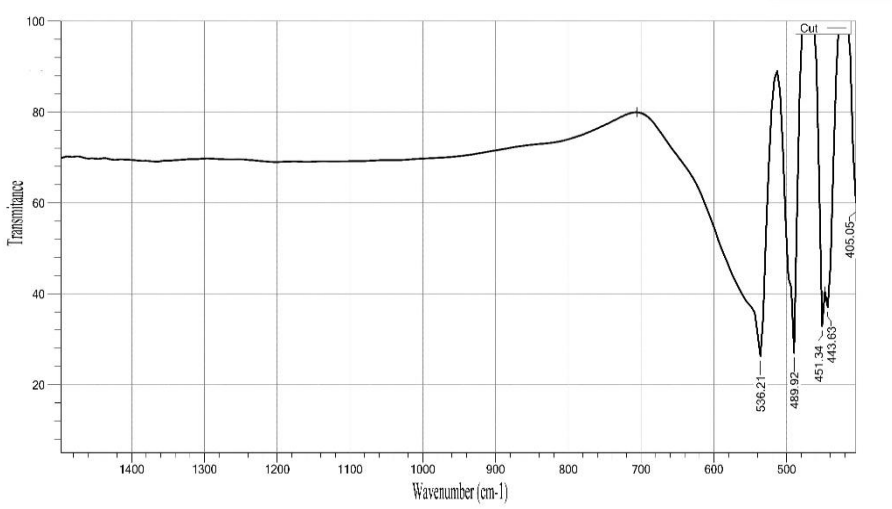


(B) Procedure 2 **(**strong peck: 526.49. 482.2, 497.63, 459.06, 439.77, 408.91)



(C) Procedure 3 **(**strong peck: 532.35, 459.06, 482.2, 497.63, 435.91, 408.91).

Annals of R.S.C.B., ISSN:1583-6258, Vol. 25, Issue 6, 2021, Pages. 14801 - 14819
Received 25 April 2021; Accepted 08 May 2021.



(D) Procedure 4 **(**strong peck: 536.21, 489.92, 451.34, 443.63 and 405.05)

Fig. (3): FT-IR spectra of $CoFe_2O_4$ synthesis by procedure (1 to 4) of crude plant extract.

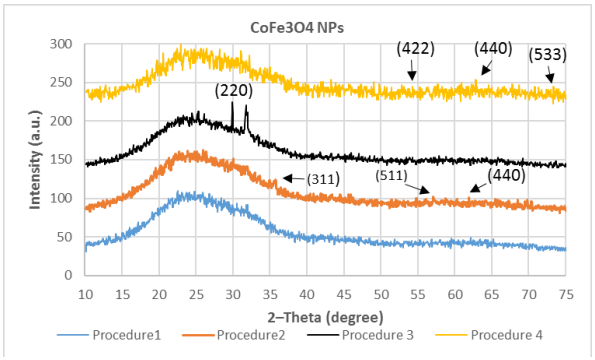


Fig. (4): X-ray pattern of $CoFe_2O_4$ of procedure (1-4)

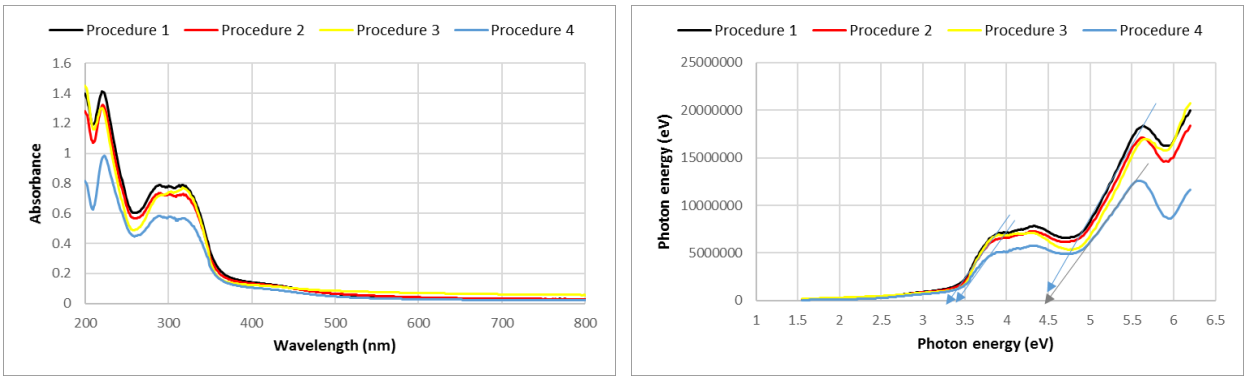
Table (2): summary of X-ray characterization of $CoFe_2O_4$ phytosynthesis nanoparticles synthesis by various plant extracts and Aspartic acid.

Sample	Planes (hkℓ)	2 theta (DEG)	FWHM (DEG)	D (nm)	STRAIN XE-4	DIS X1014
Procedure 1	220	30.6	2.329	3.947	351.15	641.88
	311	35.163	0.556	17.417	79.58	32.97
	400	43.2	0.09	120.862	11.47	0.68
Average				47.41		
Procedure 2	220	30.15	1.465	6.245	221.95	256.45
	311	35.79	1.255	7.781	178.12	165.17
	400	43.4	0.09	121.265	11.43	0.68

Annals of R.S.C.B., ISSN:1583-6258, Vol. 25, Issue 6, 2021, Pages. 14801 - 14819
Received 25 April 2021; Accepted 08 May 2021.

Average				45.1		
Procedure 3	220	30.908	0.669	13.789	100.52	52.6
	311	35.343	0.571	17.015	81.46	34.54
	400	43.3	0.09	121.063	11.45	0.68
Average				50.62		
Procedure 4	220	30.918	0.487	18.933	73.2	27.9
	311	35.35	0.652	14.895	93.06	45.08
	511	57.62	0.152	98.183	14.12	1.04
Average				44		

(hkℓ) planes: crystallographic plane; FWHM: Full width at half maximum; D: dimension of Crystal in nm; η x10^{-4}: strain value; δ x 10^{14}: dislocation density; NPs: nanoparticles; BPs: particles.



(A) (B)

Fig. (5): (A) absorptions spectrum and (B) $(ahv)^2$ versus photon energy of phytosynthesis $CoFe_2O_4$ NPs using procedures 1-4 of crude plant extract, note that procedure 6 include Aspartic acid with crude extract.

Current results approved that *R. ribes* contain six compounds: Emodin (38.25 %), Physcion (29.145 %), Rutin (13.193 %), Rhein (6.53 %) and Aloe -emodin (2.58 %). Several studies were close related to this result, Keser and his team in (2020) and (Abdul Jalill, *et al.*, 2015) found most of these compounds in stems and rhizomes respectively. Other constituents that have been also isolated from *Rheum species* are: anthocyanins, flavonoids, dianthrones, stilbenes, anthraglycosides, chromone glycosides, polyphenols, organic acids, essential oil and vitamins (Keser *et al.*, 2020).

Current results approved that methanol crude extract success to produce $CoFe_2O_4$ in nano size in three different procedures. This ability may be due to Phenolic compounds which possess hydroxyl and ketone groups that are capable of binding to metals and showing chelation (Nasrollahzadeh *et al.*, 2019). One of these Phenols was Rutin (as proven in HPLC analysis in the current study). This compound are capable to reduction of zinc salt to ZnO NPs (Bharathi and Bhuvaneshwari, 2019) it act as ligation agents and the aromatic hydroxyl groups of Rutin

Annals of R.S.C.B., ISSN:1583-6258, Vol. 25, Issue 6, 2021, Pages. 14801 - 14819
Received 25 April 2021; Accepted 08 May 2021.

react readily with tin ions, which lead to the formation of a stable complex of SnO2 nanoparticles (Suresh *et al*., 2020; Senthilkumar and sami, 2014).

Preparation of NPs using these approaches is environmentally friendly and provides NPs with better defined sizes, morphologies, and stability (Nasrollahzadeh *et al.*, 2019). Several studies were close to present plant, which approve their ability of *R. ribes* to produce silver nanoparticles (26 nm) (Zhang and Liu, 2004). In addition, *Rheum turkestanicum* (RT) has been utilized as the stabilizing agent to form fine zinc oxide nanoparticles with a size of 17-20 nm (Nemati *et al*., 2019). The fruits of another species of *Rheum* (*Ribes khorassanicum*) served as the reducing and capping agents in biosynthesis of AgNPs (Yazdi *et al*., 2018; Adibi *et al*., 2007).

Conclusions and Recommendations

Rhizomes of Iraqi *Rheum ribes* extract contain seven compounds of flavonoids. Four procedures were used to synthesis $CoFe_2O_4$ nanoparticles using methanol crude extract of Rhizomes of Iraqi *R. ribes*. The results conclude that three of those four procedures were success to produce $CoFe_2O_4$ in nano size, there were: (1, 2, 3) procedures, while procedure 4 was fail to produce nanoparticles. Studying the role of some active constituents of *Rheum sp.* in phytosynthesis of cobalt ferrite nanoparticles will be benefit.

Acknowledgments

The authors would like to thank Al-Mustansiriyah University (www. uomustansiriyah.edu.iq) Baghdad Iraq for its support in the present work.

References

1. Abdul Jalill, D. R. D. A., Hussin, M. F., and AL-Shammari, D. A. M. (2015). GC/MS Analysis of *Rheum ribes* rhizomes. Mintage J Pharma Med Sci, 1, 29-34.
2. Abdul Jalill, R. D. A. (2018). Green synthesis of titanium dioxide nanoparticles with volatile oil of Eugenia caryophyllata for enhanced antimicrobial activities. IET nanobiotechnology, 12(5), 678-687.
3. Adibi, F., Ejtehadi, H., Abrishamchi, P.: 'Phytochemicals and antibacterial effects of *Ribes khorassanicum* Saghafi and Assadi, an endemic plant species to North–East of Khorasan', J. Med. Plants, 2007, 4, (24), pp. 64–73.
4. Andersen, H. L., and Christensen, M. (2015). In situ powder X-ray diffraction study of magnetic CoFe2O4 nanocrystallite synthesis. Nanoscale, 7(8), 3481–3490.
5. Andiç, S., Tunçtürk, Y., Ocak, E., and Köse, S. (2009). Some Chemical Characteristics of Edible Wild Rhubarb Species (*Rheum ribes L.*), Research J of Agriculture and Biological Sciences, 5(6): 973-977.
6. Ansari, S. M., Bhor, R. D., Pai, K. R., Mazumder, S., Sen, D., Kolekar, Y. D., and Ramana, C. V. (2016). Size and Chemistry Controlled Cobalt-Ferrite Nanoparticles and Their Anti-proliferative Effect against the MCF-7 Breast Cancer Cells. ACS Biomaterials Science & Engineering, 2(12), 2139–2152.
7. Ba-Abbad, M.M., Kadhum, A.H., Mohamad, A.B., *et al*. (2012). 'Synthesis and catalytic activity of TiO2 nanoparticles for photochemical oxidation of concentrated chlorophenols under direct solar radiation', Int. J. Electrochem. Sci., 7, pp. 4871–4888.
8. Baker, S,, Rakshith, D., Kavitha, K. S. *et al*. (2013). "Plants: emerging as nanofactories towards facile route in synthesis of nanoparticles" BioImpacts, vol. 3, no. 3, pp. 111–117.

Annals of R.S.C.B., ISSN:1583-6258, Vol. 25, Issue 6, 2021, Pages. 14801 - 14819
Received 25 April 2021; Accepted 08 May 2021.

9. Bharathi, D., and Bhuvaneshwari, V. (2019). Synthesis of zinc oxide nanoparticles (ZnO NPs) using pure bioflavonoid rutin and their biomedical applications: antibacterial, antioxidant and cytotoxic activities. Research on Chemical Intermediates.
10. Brigger, I., Dubernet, C. and Couvreur, P. (2002). Nanoparticles in cancer therapy and diagnosis. Adv Drug Deliv Rev 54:631–651.
11. Cullity, B.D. 'Elements of X-ray diffraction' (Addison Wesley, London, 1978, 2nd edn.), p. 531.
12. Dang, T. M. D., Le, T. T. T., Fribourg-Blanc, E. and Dang, M. C. (2012). "Influence of surfactant on the preparation of silver nanoparticles by polyol method," Adv. Nat. Sci.: Nanosci. Nanotechnol. 3. 035004 (4pp).
13. Dey, C., Ghosh, A., Ahir, M., Ghosh, A. and Goswami, M.M. (2018). Improvement of Anticancer Drug Release by Cobalt Ferrite Magnetic Nanoparticles through Combined pH and Temperature Responsive Technique. Chemphyschem. Nov 5; 19(21):2872-2878.
14. Gore, S. K., Jadhav, S. S., Jadhav, V. V., Patange, S. M., Naushad, Mu., Mane, R. S. and Kim, K. H. (2017). The structural and magnetic properties of dual phase cobalt ferrite, Scientific Reports 7, Article number: 2524.
15. Grice, H.C. (1986). Safety evaluation of butylated hydroxytoluene (BHT) in the liver, lung and gastrointestinal tract. Food Chemistry and Toxicology 24, 1127–1130.
16. Issa, B.; Obaidat, I. M.; Albiss, B. A. and Haik, Y. (2013). Magnetic Nanoparticles: Surface Effects and Properties Related to Biomedicine Applications. Int J Mol Sci. 14(11): 21266–21305.
17. Jia, Z., Ren, D. and Zhu, R. (2012). "Synthesis, characterization and magnetic properties of CoFe2O4 nanorods," Materials Letters, vol. 66, no. 1, pp. 128–131.
18. Jobst, P.J., Stenzel, O., Schürmann, M., Modsching, N., Yulin, S., Wilbrandt, S., Gäbler, D., Kaiser, N. and Tünnermann, A. (2013). Optical properties of unprotected and protected sputtered silver films: Surface morphology vs. UV/VIS reflectanceAdvances in Optical Technologies. 3: 91-102.
19. Keser, S., Keser, F., Karatepe, M., Kaygili, O., Tekin, S., Turkoglu, I., and Sandal, S. (2020). Bioactive contents, In vitro antiradical, antimicrobial and cytotoxic properties of rhubarb (*Rheum ribes L.*) extracts. Natural product research, 34(23), 3353-3357.
20. Kombaiah, K.; Vijaya, J. J.; Kennedy, L. J.; Bououdina, M.; Ramalingam, R. J. and Al-Lohedan, H.A. (2018). Okra extract-assisted green synthesis of CoFe2O4 nanoparticles and their optical, magnetic, and antimicrobial properties. Materials Chemistry and Physics 204. 410e419.
21. Liu, L. Yuan, S., Long, Y., Guo, Z., Sun Y. and Li, Y. (2009). "Immunomodulation of *Rheum tanguticum* polysaccharide (RTP) on the immunosuppressive effects of dexamethasone (DEX) on the treatment of colitis in rats induced by 2,4,6-trinitrobenzene sulfonic acid," International Immunopharmacology, vol. 9, pp. 1568-1577.
22. Lu, L. T., Dung, N. T., Tung, L. D., Thanh, C. T., Quy, O. K., Chuc, N. V., Maenosono, S. and Thanh, N. T. K. (2015). Synthesis of magnetic cobalt ferrite nanoparticles with controlled morphology, monodispersity and composition: the influence of solvent, surfactant, reductant and synthetic conditions, *Nanoscale, 7(46), 19596–19610.*
23. Marslin, G., Siram, K., Maqbool, Q., Selvakesavan, R., Kruszka, D., Kachlicki, P., and Franklin, G. (2018). Secondary Metabolites in the Green Synthesis of Metallic Nanoparticles. Materials, 11(6), 940.

Annals of R.S.C.B., ISSN:1583-6258, Vol. 25, Issue 6, 2021, Pages. 14801 - 14819
Received 25 April 2021; Accepted 08 May 2021.

24. Mathew, D. S. and Juang, R.-S. (2007). "An overview of the structure and magnetism of spinel ferrite nanoparticles and their synthesis in microemulsions," Chemical Engineering J., vol. 129, no. 1–3, pp. 51–65.
25. Mericli, A. H. and Tuzlaci, E. (1990). Constituents of *Rheum ribes*. Fitoterapia. Vol.61 No.4 pp.375 ref.2.
26. Nasrollahzadeh, M., Atarod, M., Sajjadi, M., Sajadi, S. M., and Issaabadi, Z. (2019). Plant-Mediated Green Synthesis of Nanostructures: Mechanisms, Characterization, and Applications. An Introduction to Green Nanotechnology, 199–322.
27. Naveen, H. K. S., Kumar, G., Karthik, L., *et al*. (2010). 'Extracellular biosynthesis of silver nanoparticles using the filamentous fungus *Penicillium sp*.', Arch. Appl. Sci. Res., 2, (6), pp. 161–167.
28. Nemati, S., Hosseini, H. A., Hashemzadeh, A., Mohajeri, M., Sabouri, Z., Darroudi, M., and Kazemi Oskuee, R. (2019). Cytotoxicity and photocatalytic applications of biosynthesized ZnO nanoparticles by *Rheum turketanicum* rhizome extract. Materials Research Express.
29. Okwunodulu, F. U., Chukwuemeka-Okorie, H. O. and Okorie, F. C. (2019). Biological Synthesis of Cobalt Nanoparticles from *Mangifera indica* Leaf Extract and Application by Detection of Manganese (II) Ions Present in Industrial Wastewater. Chemical Science International J. 27(1): 1-8.
30. Pannaparayil, T., Marande, R., Komarneni, S. and Sankar, S.G. (1988). A novel low-temperature preparation of several ferrimagnetic spinels and their magnetic and Mössbauer characterization. *J. Appl. Phys.* 64, 5641 1988.
31. Park, B. J., Choi, K. H., Nam, K. C., Ali, A., Min, J. E., Son, H., Uhm, H. S., Kim, H. J., Jung, J. S. and Choi, E. H. (2015). Photodynamic Anticancer Activities of Multifunctional Cobalt Ferrite Nanoparticles in Various Cancer Cells. J Biomed Nanotechnol. 11(2):226-35.
32. Pathak, A. and Pramanik, P. (2001). "Nano-particles of oxides through chemical methods," Proceedings of the Indian National Science Academy, vol. 67, no. 1, pp. 47–70.
33. Prabhakaran, T. and Hemalatha, J. (2016). Combustion synthesis and characterization of cobalt ferrite nanoparticles, Ceram. Int. 4 14113–14120.
34. Rana, S., Philip, J. and Raj, B. (2010). Micelle based synthesis of cobalt ferrite nanoparticles and its characterization using Fourier Transform Infrared Transmission Spectrometry and Thermogravimetry, Mater. Chem. Phys. 124. 264-269.
35. Raval, A., Panchal, N., and Jotania, R. (2013). Structural properties and microstructure of cobalt ferrite particles synthesized by a Sol-Gel auto combustion method. In International J. of Modern Physics: Conference Series. Vol. 22, pp. 558-563.
36. Routray, K. L., Saha, S., Sanyal, D. and Behera, D. (2018). Role of rare-earth (Nd^{3+}) ions on structural, dielectric, magnetic and Mossbauer properties of nano-sized $CoFe_2O_4$: useful for high frequency application. Mater. Res. Expr. **6**, 026107.
37. Senthilkumar, M. and Sami V. N. (2014). Development and validation of GC–MS methods for determination of leaf and root of *Delonix elata* (L.) gamble. Int J Adv Res Biol Sci 1(2):93–107
38. Singh, A., Gangwar, H., and Dehiya, B. S. (2017). Synthesis and microstructural characterization of pure cobalt ferrite for DC electrical study. J Mater Sci Mech Eng, 4, 136-141.
39. Somorjai, G. A. and Park, J. Y. (2008). "Colloid science of metal nanoparticle catalysts in 2D and 3D structures. Challenges of nucleation, growth, composition, particle shape, size control

and their influence on activity and selectivity," Topics in Catalysis, vol. 49, no. 3-4, pp. 126–135.
40. Suresh, K. C., Surendhiran, S., Manoj Kumar, P. *et al.* (2020). Green synthesis of SnO2 nanoparticles using *Delonix elata* leaf extract: Evaluation of its structural, optical, morphological and photocatalytic properties. SN Appl. Sci. 2, 1735.
41. Tanrikut, E. S., Çeken, B., Altaş, S., Pirinççioğlu, M., Kizil, G., and Kizil, M. (2013). DNA cleavage protecting activity and in vitro antioxidant potential of aqueous extract from fresh stems of *Rheum ribes*. Acta Alimentaria, 42(4), 461–472.
42. Tartik, M.; Darendelioglu, E.; Aykutoglu, G. and Baydas, G. (2015). The various biological activities of *Rheum ribes* extract on different types of cell. Tr. J. Nature Sci. 2015 Vol. 4 No.
43. Tatarchuk, T., Bououdina, M., Macyk, W., Shyichuk, O., Paliychuk, N., Yaremiy, I., AlNajar, B. and Pacia, M. (2017). Structural, Optical, and Magnetic Properties of Zn-Doped CoFe2O4 Nanoparticles, Nanoscale Res. Lett. 12, 141-152.
44. Tauc, J. (1974). Amorphous and Liquid Semiconductor, Plenum, New York, p. 159.
45. Thakkar, K.N., Mhatre, S.S. and Parikh, R.Y. (2010). Biological synthesis of metallic nanoparticles. Nanomed Nanotechnol Biol Med.; 6:257–62.
46. Tran, N. and Webster, T.J. (2010). Magnetic nanoparticles: biomedical applications and challenges. J Mater Chem 20:8760–8767.
47. Tuzlaci, E. and Mericli, A. H. (1992): Some studies on Isgin (*Rheum ribes*.) and its distribution in Turkey. In: Baser KCH, ed. Proceedings of the IX Symposium on Plant Drugs. Eskisehir: Publication of Anadolu University, No. 641, pp. 336–341.
48. Tuzlacı, E. and Meriçli, A.H. (1991). Some studies on Isgın (*Rheum ribes*) and its distribution in Turkey. Proceeding of the 9th Symposium on Plant Drugs, Eskisehir, Turkey. pp. 336-341.
49. Uyar, P., Coruh, N. and Iscan, M. (2014). Evaluation of in vitro antioxidative, cytotoxic and apoptotic activities of *Rheum ribes* ethyl acetate extracts. J Plant Sci 2:339
50. Varma, P. C. R., Manna, R. S., Banerjee, D., Varma, M. R., Suresh, K. G., and Nigam, A. K. (2008). Magnetic properties of CoFe2O4 synthesized by solid state, citrate precursor and polymerized complex methods: A comparative study. J of Alloys and Compounds, 453(1-2), 298–303.
51. Wang, C. and Sun, S. (2007). Chemical Synthesis of Monodisperse Magnetic Nanoparticles. Handbook of Magnetism and Advanced Magnetic Materials.
52. Wang, H., Liu, D., Li, Y., and Duan, Q. (2016). Single-spinneret electrospinning fabrication of CoFe2O4 nanotubes as high-performance anode materials for lithium-ion batteries. Materials Letters, 172, 64–67.
53. Wang, Y. and Herron, N. (1991). Nanometer-sized semiconductor clusters: materialssynthesis, quantum size effects, and photophysical properties. J Phys Chem. 95, 525.
54. Wang, Y.; Feng, W.; Yang, F.; Zhang, Q.; Ji, L.; Li, D. and Wang, Z. (2012). Determination of four anthraquinones in Sanhuang tablets by QAMS. Zhongguo Zhong Yao Za Zhi, 37, 212–217.
55. Wei, W.; Mao, X.; Ortiz LA. and Sadoway, D. R. (2011). Oriented silver oxide nanostructures synthesized through a template-free electrochemical route. J. Materials Chemistry. 21 (2): 432–438.

Annals of R.S.C.B., ISSN:1583-6258, Vol. 25, Issue 6, 2021, Pages. 14801 - 14819
Received 25 April 2021; Accepted 08 May 2021.

56. Wichi, H. P. (1988). Enhanced tumour development by butylated hydroxyanisole (BHA) from the prospective of effect on forestomach and oesophageal squamous epithelium. Food Chemistry and Toxicology 26, 717–723
57. Yáñez-Vilar, S., Sánchez-Andújar, M., Gómez-Aguirre, C., Mira, J., Señarís-Rodríguez, M. A., Castro-García, S. (2009). A simple solvothermal synthesis of MFe_2O_4 (M = Mn, Co and Ni) nanoparticles. J. Solid State Chem. 182(10), 2685–2690.
58. Yazdi, M. E. T., Khara, J., Housaindokht, M., Sadeghnia, H. R., Esmaeilzadeh Bahabadi, S., Amiri, M. S., and Darroudi, M. (2018). Role of *Ribes khorasanicum* in the biosynthesis of silver nanoparticles and their antibacterial properties. IET Nanobiotechnology.
59. Zhang, H. X. and Liu, M. C. (2004). Separation procedures for the pharmacologically active components of rhubarb, J. Chromatogr. B, 812 175-181.